Original Article

Improved visualization of electron-density dual-energy computed tomography for lumbar disc disease over the standard gray-scale type and virtual noncalcium imaging

Pengfeng Sun[1]^, Xiaoping Wu[1], Ming Gao[1], Xiaoyue Zhang[2], Duo Ma[1], Hongsheng Liu[1], Qiaoying Zhang[1], Jiayu Wu[1], Mingyue Ma[1], Yan Dong[1], Run Liu[1]^

[1]Department of Radiology, The Affiliated Xi'an Central Hospital of Xi'an Jiaotong University, Xi'an, China; [2]Department of Clinical Science, Philips Healthcare China, Xi'an, China

Contributions: (I) Conception and design: P Sun, X Wu, R Liu, X Zhang; (II) Administrative support: X Wu, M Ma, Y Dong; (III) Provision of study materials or patients: P Sun, M Gao, D Ma; (IV) Collection and assembly of data: P Sun, D Ma, H Liu, Q Zhang, M Ma, Y Dong, R Liu; (V) Data analysis and interpretation: P Sun, D Ma, J Wu; (VI) Manuscript writing: All authors; (VII) Final approval of manuscript: All authors.

Correspondence to: Run Liu, MD. Department of Radiology, The Affiliated Xi'an Central Hospital of Xi'an Jiaotong University, No. 161, West 5th Road, Xi'an 710003, China. Email: runliulgl@163.com.

Background: Dual-energy computed tomography (DECT) enhances tissue imaging characterization. However, no studies have evaluated the diagnostic accuracy of electron density (ED) for simultaneously displaying the lumbar disc and disc calcification. This retrospective study aimed to investigate the ability of ED to visualize lumbar disc disease as compared with standard computed tomography (SC) and virtual noncalcium (VNCa) imaging in order to provide a viable alternative for lumbar disc disease.

Methods: From October 2023 to February 2024, we retrospectively analyzed data from 53 patients who underwent DECT and 3.0-T magnetic resonance imaging (MRI) within 2 weeks. The randomized SC, VNCa, and ED image sets were independently evaluated by four radiologists for visualization of the lumbar disc and disc calcification with an 8-week interval. Final disc calcification results were obtained by consensus, with the SC results serving as the reference standard. Two other experienced radiologists performed MRI evaluations as the lumbar disc reference standard. Diagnostic performance was compared for each image.

Results: Among the 298 included lumbar discs, 183 lumbar disc herniations and bulges were revealed on MRI. As compared with VNCa and SC, ED showed higher overall sensitivity (91.3% *vs.* 88.9% *vs.* 78.0%), specificity (94.8% *vs.* 93.3% *vs.* 88.0%), and accuracy (92.6% *vs.* 90.6% *vs.* 81.9%) in visualizing lumbar disc herniation and bulging. The ED area under the curve (AUC) was higher than that of VNCa and SC (all P values <0.05), and ED identified all 40 (40/183) calcified discs shown on SC. In addition, diagnostic confidence and image quality of ED were higher than those of VNCa and SC (all P values <0.001).

Conclusions: ED demonstrated higher diagnostic accuracy and confidence for visualizing the lumbar disc and disc calcification on the computed tomography (CT) images as compared to VNCa and SC.

Keywords: Dual-energy computed tomography (DECT); intervertebral disc disease; magnetic resonance imaging (MRI); lumbar vertebrae; disc calcification

Submitted Aug 24, 2024. Accepted for publication Jan 20, 2025. Published online Feb 26, 2025.
doi: 10.21037/qims-24-1760
View this article at: https://dx.doi.org/10.21037/qims-24-1760

^ ORCID: Pengfeng Sun, 0009-0005-0322-3052; Run Liu, 0009-0008-1385-7528.

Introduction

Lumbar disc herniation and bulging often result in numbness, lower limb pain, and lower back pain (1,2), all of which are common indications for spinal surgery. In addition, disc calcification, a usually disregarded disc phenotype, may significantly impact clinical outcomes. Cadaveric radiographic studies have shown that the occurrence rate of calcified discs in adults varies from 5% to 71% (3-5). Calcified discs are more likely to rupture and herniate than are noncalcified discs. In addition, they are usually more symptomatic and display larger herniations, presenting a surgical challenge (6-8). Therefore, prompt detection of lumbar disc bulging and herniation, whether calcified or not, is essential for ensuring optimal treatment and preventing complications.

Magnetic resonance imaging (MRI) is the ideal imaging technique for disc disorders because it provides a contrast between cerebrospinal fluid and intervertebral discs (9). However, MRI has its own limitations. For instance, pacemakers and cochlear implants are contraindication, as are claustrophobia and the inability to lie still. In addition, MRI has a limited capacity to visualize disc calcification. Standard computed tomography (SC) can readily demonstrate calcification but has limited capacity to demonstrate disc herniation (10). Therefore, there is a clinical need to develop a technique that can display both the intervertebral disc and calcification clearly on the same image.

Dual-energy computed tomography (DECT) enhances tissue characterization by virtue of its material decomposition capability (11-13). One study reported that DECT could detect vertebral bone marrow edema associated with vertebral fractures with high specificity, avoiding the need for confirmatory MRI in emergent situations (14). In addition, virtual noncalcium (VNCa) imaging in DECT can demonstrate disc herniation better than can SC and has similar diagnostic capabilities as those of MRI (15-17). Electron density (ED) indicates the likelihood of an electron being at a particular location and is influenced by the molecular structure of the tissue. Virtual monoenergetic DECT images allow for the direct calculation of ED in tissues through measurement of X-ray attenuation at two distinct energies and may suggest cellularity (18,19). The ED value obtained from DECT is shown as a percentage as compared to the ED of water (%EDW). One study reported the high validity of ED estimation based on DECT, and it thus has the potential to improve the procedural ease and accuracy of measuring ED in clinical practice (18). ED is commonly associated with the physical density of tissues. Clinically, it is applied to optimize radiotherapy dose distribution rather than for diagnostic purposes. Recently, one study concluded that ED imaging could better detect cervical disc herniation than could VNCa or SC (20). In contrast to solely detecting intervertebral discs, identifying both intervertebral discs and disc calcification within the same image presents a more complex challenge. ED has a correlation with mass density and computed tomography (CT) Hounsfield unit (HU) values (21). The CT HU values for intervertebral disc tissue and calcification exhibit significant variability; moreover, the HU values for calcification are consistently higher than those for disc tissue. Thus, ED may perhaps serve as a novel technique for visualizing intervertebral disc disease. We hypothesized that ED derived from DECT can help visualize the lumbar disc and disc calcification on the same CT image.

Currently, no studies have evaluated ED's diagnostic accuracy in simultaneously demonstrating the lumbar disc and disc calcification. Therefore, in this study, we compared the diagnostic accuracy of ED in visualizing the lumbar disc and disc calcification with that of SC and VNCa. We present this article in accordance with the STARD reporting checklist (available at https://qims.amegroups.com/article/view/10.21037/qims-24-1760/rc).

Methods

This study was conducted in accordance with the Declaration of Helsinki (as revised in 2013) and was approved by the Institutional Review Board (IRB) of The Affiliated Xi'an Central Hospital of Xi'an Jiaotong University (No. LW-2024-04). The requirement for individual consent was waived due to the retrospective nature of the analysis.

Patient selection and study design

Eighty consecutive patients underwent noncontrast spectral CT and 3.0-T MRI of the lumbar spine within 2 weeks in routine clinical visits between October 2023 and February 2024. Patients with known spinal malignancy, fractures, intervertebral spacers, and dorsal instrumentation were excluded. Consequently, lumbar discs in 53 patients were evaluated from the T12/L1 to the L5/S1 vertebrae (6 levels), with 20 discs excluded due to a lack of DECT data. The final data included 298 lumbar discs from 53 patients (*Figure 1*).

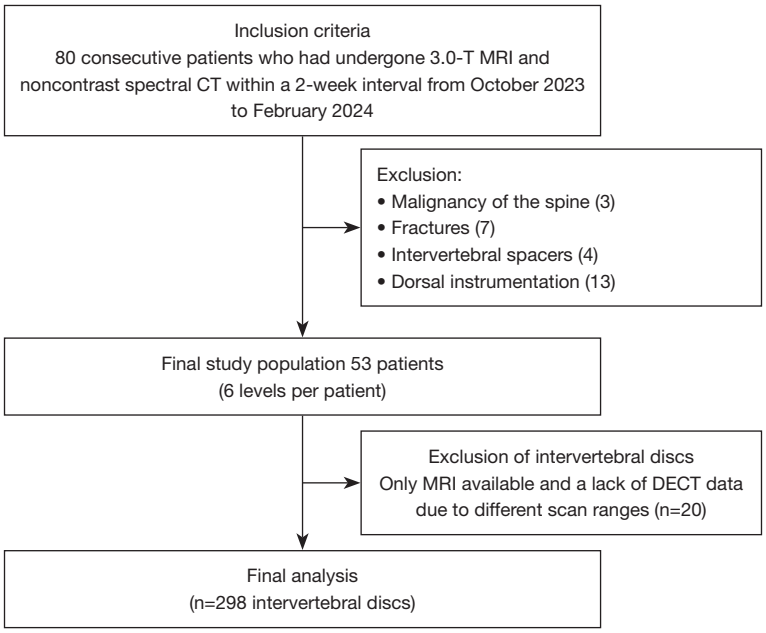

Figure 1 Flowchart of the study population selection. MRI, magnetic resonance imaging; CT, computed tomography; DECT dual-energy computed tomography.

DECT scan protocol

Noncontrast CT scans of the lumbar spine were performed using a commercial dual-energy spectral CT scanner (Spectral CT 7500, Philips Healthcare, Best, the Netherlands). Patients were scanned in a craniocaudal direction under the following parameters: pitch, 0.60; rotation time, 0.75 s; collimation, 128×0.625 mm; slice thickness, 1 mm; increment, 1 mm; and three-dimensional (3D) tube current modulation. The mean volume CT dose index was 11.8±3.0 mGy (range, 6.3–17.8 mGy), and mean dose-length product was 458.4±169.0 mGy·cm (range, 178–969 mGy·cm).

Image reconstruction and postprocessing

The 3D IntelliSpace Portal workstation (V12.0; Philips Healthcare) was used for postprocessing to generate ED and VNCa images. Axial and sagittal reconstruction was performed (section thickness and increment of 1 mm). Furthermore, an original ED and VNCa visually optimized window level and width were established for analysis, with the window level and width set at 105 and 25 for ED and at 60 and 250 for VNCa, respectively. These settings were adjustable. For VNCa, the calcium suppression index was set at 65 (22), and readers were free to adjust the index.

MRI image acquisition

MRI was performed using a 3.0-T scanner with a dedicated spine surface coil (Ingenia, Philips Healthcare). The scan protocol included the following: sagittal T1-weighted (T1W) turbo spin-echo (TSE) images [matrix size, 212×296; section thickness, 4 mm; time to repetition/time to each (TR/TE) =400/9 ms], T2-weighted (T2W) TSE images (matrix size, 192×247; section thickness, 4 mm; TR/TE, 2,000/100 ms), and T2W Dixon-water images (matrix size, 224×313; section thickness, 4 mm; TR/TE, 2,000/120 ms) in the sagittal orientation. Finally, T2W TSE sequences were obtained in the axial plane.

Image analysis

The imaging evaluation was performed via the IntelliSpace Portal workstation. First, two radiologists with 19 and 25 years of musculoskeletal imaging experience, respectively, analyzed the MRI examinations. They determined the reference standard for lumbar disc herniation and bulging that was invisible to clinical and DECT information and distinguished calcified and noncalcified discs, with the aim of arriving at a consensus. The analysis of lumbar disc herniation and bulging was evaluated based on the lumbar disc pathologic classification of the North American Spine

Table 1 Patient population data (N=53)

Characteristics	Value (n=53)
Gender, n	
Female	26
Male	27
Age (years)	
Mean ± SD	64±17
Range	24–101
Patients with known lumbar disc bulging or herniation, n (%)	15 (28.3)
Patients with known osteoporosis, n (%)	7 (13.2)
Patients with known scoliosis, n (%)	5 (9.4)

SD, standard deviation.

Society (NASS) version 2.0 (23), and the characteristics were described as follows: bulging, protruded, extruded, and sequestered disc morphology. Spinal nerve root impingement (grade 1, contact; grades 2–3, deviation and/or compression) due to lumbar discs was assessed based on the Pfirrmann Nerve Root Compression Grading System (24).

After the reference standard for lumbar disc herniation and bulging was determined, four radiologists with 1, 5, 6, and 20 years of musculoskeletal imaging experience, respectively, evaluated DECT sequences. They were blinded to the MRI, and clinical information that was provided in a randomized blinded fashion. Each reader was instructed to note the presence and degree of bulging or herniated discs and the presence of calcification and spinal nerve root impingement. All SC, VNCa, and ED images were randomly evaluated, with an 8-week interval between each imaging set. Finally, if the results for disc calcification were inconsistent, consensus was reached after re-evaluation. The SC results were recognized as the disc calcification reference standard and compared to those of VNCa and ED.

The diagnostic confidence and image quality for assessing lumbar discs for all CT series were individually rated on a 5-point scale in terms of diagnostic confidence (1= cannot diagnose, 2= low confidence in diagnosis, 3= somewhat confident in diagnosis, 4= highly confident in diagnosis, 5= absolutely confident in diagnosis) and image quality (1= unacceptable, 2= less than average, 3= average, 4= above average, 5= excellent) (25).

Statistical analysis

Statistical analyses were performed using SPSS 27.0 (IBM Corp., Armonk, NY, USA) and GraphPad Prism 10 (Dotmatics, Boston, MA, USA). Data distribution was assessed via the Kolmogorov-Smirnov test. Categorical variables are expressed as percentages, and continuous variables are expressed as the mean ± standard deviation. Using 2×2 contingency tables, we calculated the sensitivity, specificity, positive predictive value (PPV), negative predictive value (NPV), and accuracy for each method. The 95% confidence interval (95% CI) of the area under the curve (AUC) and P values were calculated with the DeLong test. The weighted Fleiss kappa coefficient was used to measure the interreader agreement for the presence of lumbar disc disease and spinal stenosis. The results of the quantitative evaluation of diagnostic confidence and image quality were visualized as violin plots, and the statistical significance was assessed via analysis of variance (ANOVA). A P value <0.05 was considered to be statistically significant.

Results

A total of 298 lumbar discs were collected from 53 patients, (mean age 64±17 years; range, 24–101 years), comprising 27 men and 26 women. Among the patients, 15 had known disc bulging or herniation, 7 had osteoporosis, and 5 had scoliosis (*Table 1*). With MRI as the reference standard, 183 lumbar disc herniations and bulges were depicted; specifically, these were classified according to the NASS as 109 bulges, 59 protrusions, and 15 extrusions. The mean examination interval between DECT and MRI was 2.4 days (range, 0–14 days).

Diagnostic accuracy for lumbar disc herniation and bulging

All lumbar disc herniation and bulging were assessed based on the NASS classification, and ED images, as compared to VNCa and SC images, showed higher overall sensitivity (91.3% *vs.* 88.9% *vs.* 78.0%), specificity (94.8% *vs.* 93.3% *vs.* 88.0%), PPV (96.5% *vs.* 95.5% *vs.* 91.2%), NPV (87.2% *vs.* 84.1% *vs.* 71.6%), and accuracy (92.6% *vs.* 90.6% *vs.* 81.9%) (with clustering being accounted for by the four readers). The AUC of ED images was higher than that of the VNCa and SC images (all P values <0.05). All the

readers demonstrated improved sensitivity and specificity in assessing ED and VNCa images as compared to SC. In addition, the ED results were consistently higher than were the VNCa ones, although the difference in AUC did not reach statistical significance (*Table 2*).

In assessing lumbar disc bulging based on the NASS classification, ED images, as compared to VNCa and SC images, demonstrated higher overall sensitivity (91.3% *vs.* 89.7% *vs.* 79.4%), specificity (95.2% *vs.* 93.0% *vs.* 86.6%), PPV (91.7% *vs.* 88.1% *vs.* 77.4%), NPV (95.0% *vs.* 94.0% *vs.* 87.9%), and accuracy (93.8% *vs.* 91.8% *vs.* 84.0%) (with clustering being accounted for by the four readers). The AUC of ED was higher than that of the VNCa and SC images (all P values <0.05). For detecting lumbar disc protrusion and extrusion, the ED results were consistently higher than those of VNCa, although the difference in AUC did not reach statistical significance (*Table 3*). As shown in *Figures 2-4*, ED could potentially enhance the detection of these conditions.

The interreader agreement for lumbar disc herniation and bulging among all four readers was substantial for the ED (κ=0.787) and VNCa (κ=0.724) images and moderate for the SC images (κ=0.502).

Diagnostic accuracy for nerve root impingement

For depicting spinal nerve root impingement, the ED images, as compared with VNCa and SC images, showed higher overall sensitivity (92.7% *vs.* 88.7% *vs.* 74.2%), specificity (99.4% *vs.* 98.9% *vs.* 97.6%), PPV (95.0% *vs.* 90.2% *vs.* 78.0%), NPV (99.2% *vs.* 98.7% *vs.* 97.0%), and accuracy (98.7% *vs.* 97.8% *vs.* 95.1%) (with clustering being accounted for). The AUC of the ED images was higher than that of the VNCa and SC images (all P values <0.05) (*Table 4*). Analysis by the individual readers revealed improved sensitivity and specificity in the ED and VNCa images as compared with SC. In addition, the ED results were consistently higher than those of VNCa, although the difference in AUC did not reach statistical significance (*Table 4*).

The interreader agreement for spinal nerve root impingement calculated among all four readers was excellent for the ED (κ=0.917) and VNCa (κ=0.854) images and substantial for the SC images (κ=0.737).

Diagnostic accuracy for lumbar disc calcification

Of the 183 herniated and bulging lumbar discs revealed on SC images, 40 (21.9%) had disc calcification, including 14 bulges, 20 protrusions, and 6 extrusions. ED detected all cases of disc calcification, demonstrating high densities, as did SC. However, disc calcification subtracted on VNCa appeared as areas with varying degrees of black (35/40), likely representing disc gas accumulation (*Figures 3*,*4*), or as areas slightly white in color in smaller patients (5/40). In addition, the calcified and noncalcified discs could not be distinguished on MRI by two radiologists.

Diagnostic confidence and image quality assessments

Compared to VNCa and SC, ED demonstrated significantly higher levels of diagnostic confidence and image quality for lumbar disc herniation and bulging (all P values <0.001) (*Figure 5*). The mean diagnostic confidence scores for the SC, VNCa, and ED images were 3.01, 4.07, and 4.87, respectively. Interreader agreement was found to be substantial for the SC (κ=0.615) and VNCa (κ=0.769) images and excellent for the ED images (κ=0.838). Similarly, the mean image quality scores for the SC, VNCa, and ED images were 3.0, 4.09, and 4.90, respectively, with substantial interreader agreement for the SC (κ=0.689) and VNCa (κ=0.760) images and excellent agreement for the ED images (κ=0.835).

Discussion

We assessed the value of the ED technique in visualizing the lumbar disc and disc calcification. Our findings demonstrated that ED simultaneously visualized the lumbar disc and disc calcification, enabling clear observation of their spatial relationship. Lumbar disc lesions are a common cause of lower back pain, particularly in middle-aged and older adult individuals, and the herniated or bulging disc may also be calcified, making treatment more difficult. MRI provides excellent disc visualization but poor visualization of disc calcification. In contrast, SC is effective at identifying disc calcification but lacks clarity in visualizing the intervertebral disc.

Applying ED images for visualizing discs has demonstrated significantly higher diagnostic accuracy and confidence for assessing cervical disc herniation than has using SC and VNCa images (20). However, ED imaging may produce false-negative and false-positive disc lesions, suggesting that while ED imaging reduces noise and provides accurate density values, it may be susceptible to miscalculation due to CT artifacts. Our findings further support the superiority of ED images for detecting lumbar

Table 2 Comparison of diagnostic accuracy of all readers for the detection of lumbar disc disease per intervertebral disc

Statistical analysis	SC	VNCa	ED	P value		
				SC *vs.* VNCa	VNCa *vs.* ED	SC *vs.* ED
Average				<0.001	0.018	<0.001
Sensitivity (%)	78.0 (571/732) [75–81]	88.9 (651/732) [86–91]	91.3 (668/732) [89–93]			
Specificity (%)	88.0 (405/460) [85–91]	93.3 (429/460) [91–95]	94.8 (436/460) [92–96]			
PPV (%)	91.2 (571/626) [89–93]	95.5 (631/682) [94–97]	96.5 (668/692) [95–98]			
NPV (%)	71.6 (405/566) [68–75]	84.1 (429/510) [81–87]	87.2 (436/500) [84–90]			
Accuracy (%)	81.9 (976/1,192) [80–84]	90.6 (1,080/1,192) [89–92]	92.6 (1,104/1,192) [91–94]			
AUC (%)	83 [81–85]	91 [90–93]	93 [92–95]			
Reader 1				<0.001	0.162	<0.001
Sensitivity (%)	70.0 (128/183) [63–76]	86.3 (158/183) [81–91]	89.1 (163/183) [84–93]			
Specificity (%)	81.7 (94/115) [74–88]	90.4 (104/115) [84–95]	92.2 (106/115) [86–96]			
PPV (%)	85.9 (128/149) [79–91]	93.5 (158/169) [89–96]	94.8 (163/172) [90–97]			
NPV (%)	63.1 (94/149) [55–70]	80.6 (104/129) [73–87]	84.1 (106/126) [77–89]			
Accuracy (%)	74.5 (222/298) [69–79]	87.9 (262/298) [84–91]	90.3 (269/298) [86–93]			
AUC (%)	76 [71–81]	88 [5–92]	91 [87–94]			
Reader 2				<0.001	0.309	<0.001
Sensitivity (%)	77.0 (141/183) [70–83]	88.0 (161/183) [82–92]	90.7 (166/183) [86–94]			
Specificity (%)	89.6 (103/115) [83–94]	93.9 (108/115) [88–97]	94.8 (109/115) [89–98]			
PPV (%)	92.2 (141/153) [87–95]	95.8 (161/168) [92–98]	96.5 (166/172) [93–98]			
NPV (%)	71.0 (103/145) [63–78]	83.1 (108/130) [76–89]	86.5 (109/126) [79–91]			
Accuracy (%)	81.9 (244/298) [77–86]	90.3 (269/298) [86–93]	92.3 (275/298) [89–95]			
AUC (%)	83 [80–88]	91 [88–94]	93 [90–96]			
Reader 3				0.002	0.351	<0.001
Sensitivity (%)	79.8 (146/183) [73–85]	89.1 (163/183) [84–93]	91.3 (167/183) [86–95]			
Specificity (%)	90.4 (104/115) [84–95]	93.9 (108/115) [88–97]	94.8 (109/115) [89–98]			
PPV (%)	93.0 (146/157) [88–96]	95.9 (163/170) [92–98]	96.5 (167/173) [93–98]			
NPV (%)	73.8 (104/141) [66–80]	84.4 (108/128) [77–90]	87.2 (109/125) [80–92]			
Accuracy (%)	83.9 (250/298) [79–88]	90.9 (271/298) [87–94]	92.6 (276/298) [89–95]			
AUC (%)	85 [81–89]	92 [88–95]	93 [90–96]			
Reader 4				0.001	0.153	<0.001
Sensitivity (%)	85.2 (156/183) [79–90]	92.3 (169/183) [88–95]	94.0 (172/183) [90–97]			
Specificity (%)	90.4 (104/115) [84–95]	94.8 (109/115) [89–98]	97.4 (112/115) [93–99]			
PPV (%)	93.4 (156/167) [89–96]	96.6 (169/175) [93–98]	98.3 (172/175) [95–99]			
NPV (%)	79.4 (104/131) [72–85]	88.6 (109/123) [82–93]	91.1 (112/123) [85–95]			
Accuracy (%)	87.2 (260/298) [83–91]	93.3 (278/298) [90–96]	95.3 (284/298) [92–97]			
AUC (%)	88 [84–92]	94 [91–96]	96 [93–98]			

Denominators represent the total number with respect to the corresponding statistical measure. Data in square brackets are the 95% CI. NPV, negative predictive value; PPV, positive predictive value; AUC, area under the curve; SC, standard computed tomography; VNCa, virtual noncalcium; ED, electron-density; CI, confidence interval.

Table 3 Diagnostic accuracy for the classification of lumbar disc disease per intervertebral disc

Statistical analysis	SC	VNCa	ED	P value		
				SC *vs.* VNCa	VNCa *vs.* ED	SC *vs.* ED
Lumbar disc bulging				<0.001	0.027	<0.001
Sensitivity (%)	79.4 (346/436) [75–83]	89.7 (391/436) [86–92]	91.3 (398/436) [88–94]			
Specificity (%)	86.6 (655/756) [84–89]	93.0 (703/756) [91–95]	95.2 (720/756) [93–97]			
PPV (%)	77.4 (346/447) [73–81]	88.1 (391/444) [85–91]	91.7 (398/434) [89–94]			
NPV (%)	87.9 (655/745) [85–90]	94.0 (703/748) [92–95]	95.0 (720/758) [93–96]			
Accuracy (%)	84.0 (1,001/1,192) [82–86]	91.8 (1,094/1,192) [90–93]	93.8 (1,118/1,192) [93–95]			
AUC (%)	83 [81–85]	91 [90–93]	93 [92–95]			
Lumbar disc protrusion				<0.001	0.143	<0.001
Sensitivity (%)	76.3 (180/236) [70, 81]	87.3 (206/236) [82–91]	90.7 (214/236) [86–94]			
Specificity (%)	94.7 (905/956) [93–96]	97.4 (931/956) [96–98]	97.5 (932/956) [96–98]			
PPV (%)	77.9 (180/231) [72–83]	89.2 (206/231) [85–93]	89.9 (214/238) [85–93]			
NPV (%)	94.2 (905/961) [93–95]	96.9 (931/961) [96–98]	97.7 (932/954) [97–98]			
Accuracy (%)	91.0 (1,085/1,192) [89–93]	95.4 (1,137/1,192) [94–96]	96.1 (1,146/1,192) [95–97]			
AUC (%)	86 [83–88]	92 [90–95]	94 [92–96]			
Lumbar disc extrusion				0.001	0.154	<0.001
Sensitivity (%)	75.0 (45/60) [63–84]	90.0 (54/60) [80–95]	93.3 (56/60) [84–97]			
Specificity (%)	100 (1,132/1,132) [99.6–100]	100 (1,132/1,132) [99.6–100]	100 (1,132/1,132) [99.6–100]			
PPV (%)	100 (45/45) [92–100]	100 (54/54) [93–100]	100 (56/56) [94–100]			
NPV (%)	98.7 (1,132/1,147) [98–99]	99.5 (1,132/1,138) [99–100]	99.6 (1,132/1,136) [99–100]			
Accuracy (%)	98.7 (1,177/1,192) [98–99]	99.5 (1,186/1,192) [99–100]	99.7 (1,188/1,192) 99–100]			
AUC (%)	88 [82–93]	95 [91–99]	97 [94–100]			

Denominators represent the total number with respect to the corresponding statistical measure. Data in square brackets are the 95% CI. PPV, positive predictive value; NPV, negative predictive value; AUC, area under the curve; SC, standard computed tomography; ED, electron-density; VNCa, virtual noncalcium; CI, confidence interval.

disc herniation, bulging, and spinal nerve root impingement in terms of sensitivity and accuracy as compared to SC and VNCa images. Furthermore, ED images provided higher diagnostic confidence and image quality as compared to VNCa or SC images, with excellent interreader agreement, along with superior visualization of the lumbar disc and disc calcification. In our study, the ED did not produce false-negative or false-positive disc lesions due to artifacts in lumbar spine examinations.

For lumbar disc herniation, gray-scale CT has demonstrated moderate diagnostic accuracy (25,26). Meanwhile, VNCa images provide better sensitivity and accuracy than do SC images (15). Although most previous studies in this area have used color-coded VNCa images, our study found that gray-scale VNCa images could aid in diagnosing lumbar disc herniation and bulging, despite having lower sensitivity and accuracy than those of ED images. In contrast to our findings, other reports suggest that VNCa images tend to be coarse and noisy in detecting cervical disc herniation (20) possibly due to artifacts in the cervical spine CT images caused by photon starvation or beam-hardening (27).

Clinically, disc calcification has been associated with poor surgical outcomes and persistent back pain that is unresponsive to conservative treatment (28,29). Although MRI offers high contrast between intravertebral fluid and

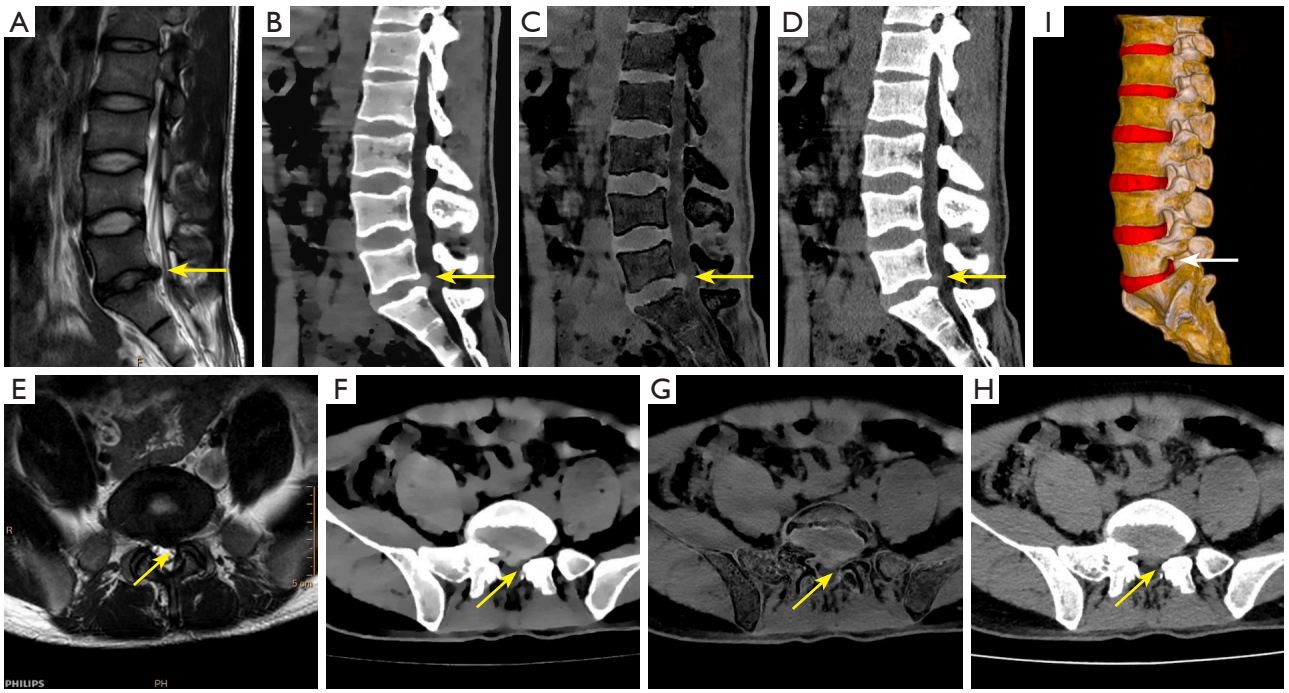

Figure 2 A 26-year-old male with lower back pain and paresthesia in the left lower leg. (A) Sagittal T2-weighted image showing lumbar disc protrusion at the L5/S1 level [yellow arrows in (A-D)]. (B) ED image providing clearer visualization of disc protrusion than (C) VNCa and (D) SC. (E) Axial T2-weighted images showing nerve root impingement [yellow arrows in (E-H)]. (F) ED providing clearer visualization than (G) VNCa and (H) SC. (I) A ED-VR showing foraminal stenosis on the left side (white arrow). ED, electron-density; VNCa, virtual noncalcium; SC, standard computed tomography; ED-VR, volume-rendering model generated from ED.

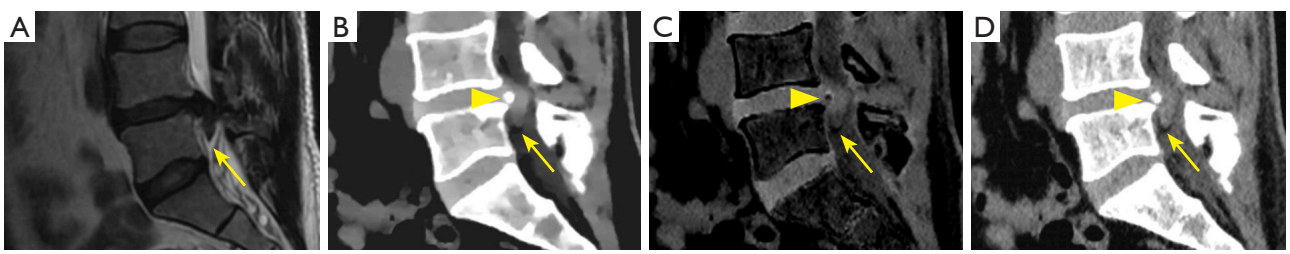

Figure 3 A 41-year-old male with the chief complaint of low back pain with radiating pain in his left leg. (A) Sagittal T2-weighted image showing lumbar disc extrusion at the L4/L5 level [yellow arrows in (A-D)]. (B) ED image providing clearer visualization compared to (C) VNCa and (D) SC. Disc calcification [yellow arrowheads in (B-D)] visible on ED and SC images but subtracted and appearing black on the VNCa image, thus being indistinguishable on sagittal T2-weighted imaging. ED, electron-density; VNCa, virtual noncalcium; SC, standard computed tomography.

discs, its ability to detect calcification is limited (30). In our study, two radiologists were unable to identify disc calcification on MRI. It is widely recognized that CT can better identify calcification than can MRI, while DECT can better distinguish materials than can SC (31). However, the VNCa technique has significant limitations in assessing calcification, as it involves subtracting calcium from anatomical structures (32). We observed that in addition to improving lumbar disc visualization, ED images are equally effective as SC in identifying disc calcification. Among the 183 herniated and bulging lumbar discs in our study, calcifications were detected in 40 discs on both SC and

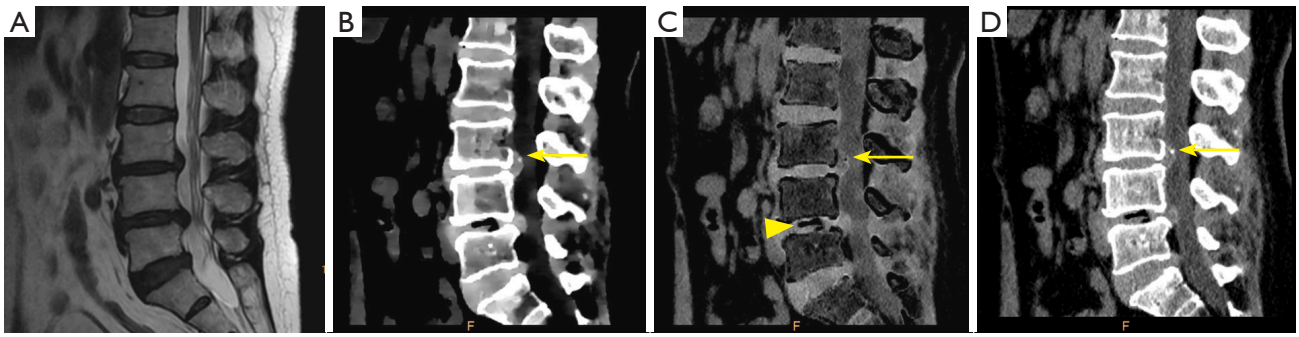

Figure 4 A 54-year-old female with left lower limb pain. (A) Sagittal T2-weighted image showing lumbar disc bulging at the L3/L4, L4/L5, and L5/S1 levels. (B) ED image providing clearer visualization compared to (C) VNCa and (D) SC. Disc calcification at the L3/L4 level [yellow arrows in (B-D)] visible on ED and SC images but subtracted and appearing black and the same as disc gas accumulation on the VNCa image [yellow arrowhead in (C)], thus being indistinguishable on sagittal T2-weighted imaging. ED, electron-density; VNCa, virtual noncalcium; SC, standard computed tomography.

Table 4 Diagnostic accuracy of all readers for nerve root display

Statistical analysis	SC	VNCa	ED	P value		
				SC *vs.* VNCa	VNCa *vs.* ED	SC *vs.* ED
Average				<0.001	0.031	<0.001
Sensitivity (%)	74.2 (92/124) [66–81]	88.7 (110/124) [82–93]	92.7 (115/124) [87–96]			
Specificity (%)	97.6 (1,042/1,068) [96–98]	98.9 (1,056/1,068) [98–99]	99.4 (1,062/1,068) [99–100]			
PPV (%)	78.0 (92/118) [70–85]	90.2 (110/122) [84–94]	95.0 (115/121) [90–98]			
NPV (%)	97.0 (1,042/1,074) [96–98]	98.7 (1,056/1,070) [98–99]	99.2 (1,062/1,071) [98–100]			
Accuracy (%)	95.1 (1,134/1,192) [94–96]	97.8 (1,166/1,192) [97–99]	98.7 (1,177/1,192) [98–99]			
AUC (%)	86 [82–90]	94 [91–97]	96 [94–98]			
Reader 1				0.01	0.129	0.002
Sensitivity (%)	64.5 (20/31) [47–79]	83.9 (26/31) [67–93]	90.3 (28/31) [75–97]			
Specificity (%)	95.5 (255/267) [92–97]	98.5 (263/267) [96–99]	98.9 (264/267) [97–100]			
PPV (%)	62.5 (20/32) [45–77]	86.7 (26/30) [70–95]	90.3 (28/31) [75–97]			
NPV (%)	95.9 (255/266) [93–98]	98.1 (263/268) [96–99]	98.9 (264/267) [97–100]			
Accuracy (%)	92.3 (275/298) [89–95]	97.0 (289/298) [94–98]	98.0 (292/298) [96–99]			
AUC (%)	80 [71–89]	91 [85–98]	95 [89–100]			
Reader 2				0.035	0.224	0.014
Sensitivity (%)	71.0 (22/31) [53–84]	87.1 (27/31) [71–95]	90.3 (28/31) [75–97]			
Specificity (%)	97.8 (261/267) [95–99]	98.9 (264/267) [97–100]	99.6 (266/267) [98–100]			
PPV (%)	78.6 (22/28) [60–90]	90.0 (27/30) [74–97]	96.6 (28/29) [83–99]			
NPV (%)	96.7 (261/270) [94–98]	98.5 (264/268) [96–99]	98.9 (266/269) [97–100]			
Accuracy (%)	95.0 (283/298) [92–97]	97.7 (291/298) [95–99]	98.7 (294/298) [97–99]			
AUC (%)	84 [76–93]	93 [87–99]	95 [90–100]			

Table 4 (*continued*)

Table 4 (*continued*)

Statistical analysis	SC	VNCa	ED	P value		
				SC *vs.* VNCa	VNCa *vs.* ED	SC *vs.* ED
Reader 3				0.027	0.527	0.011
Sensitivity (%)	77.4 (24/31) [60–89]	90.3 (28/31) [75–97]	93.5 (29/31) [79–98]			
Specificity (%)	98.1 (262/267) [96–99]	98.9 (264/267) [97–100]	99.3 (265/267) [97–100]			
PPV (%)	82.8 (24/29) [65–92]	90.3 (28/31) [75–97]	93.5 (29/31) [79–98]			
NPV (%)	97.4 (262/269) [95–99]	98.9 (264/267) [97–100]	99.3 (265/267) [97–100]			
Accuracy (%)	96.0 (286/298) [93–98]	98.0 (292/298) [96–99]	98.7 (294/298) [97–100]			
AUC (%)	88 [80–95]	95 [89–100]	96 [92–100]			
Reader 4				0.063	0.224	0.023
Sensitivity (%)	83.9 (26/31) [67–93]	93.5 (29/31) [79–98]	96.8 (30/31) [84–99]			
Specificity (%)	98.9 (264/267) [97–100]	99.3 (265/267) [97–100]	100 (267/267) [99–100]			
PPV (%)	89.7 (26/29) [74–96]	93.5 (29/31) [79–98]	100 (30/30) [89–100]			
NPV (%)	98.1 (264/269) [96–99]	99.3 (265/267) [97–100]	99.6 (267/268) [98–100]			
Accuracy (%)	97.3 (290/298) [95–99]	98.7 (294/298) [97–99]	99.7 (297/298) [98–100]			
AUC (%)	91 [85–98]	96 [92–101]	98 [95–102]			

Denominators represent the total number with respect to the corresponding statistical measure. Data in square brackets are the 95% CI. PPV, positive predictive value; NPV, negative predictive value; AUC, area under the curve; SC, standard computed tomography; ED, electron-density; VNCa, virtual noncalcium; CI, confidence interval.

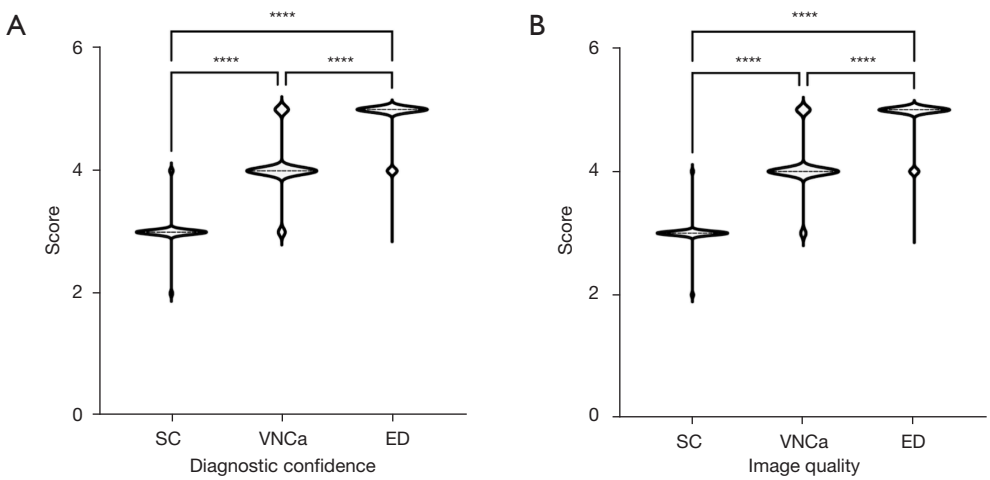

Figure 5 Violin plots for qualitative assessment of diagnostic confidence and image quality of SC, ED, and VNCa. ED achieved significantly higher scores than did VNCa and SC (all P values <0.001). ****, P<0.001. SC, standard computed tomography; ED, electron-density; VNCa, virtual noncalcium.

ED images. It should be noted that scoliosis in the lumbar spine is a common occurrence that may hinder the precise display of disc disease; the use of DECT ED data for 3D reconstruction offers a more accurate visual assessment of the lumbar disc.

The volume-rendering (VR) model can intuitively display

anatomical structures with full-depth perception. The spinal vertebrae can be visually observed via CT-VR imaging, but the disc VR model remains limited, despite findings from a few studies that have employed MR imaging (33,34). We speculate that ED images could be used to generate a VR model of the disc and spine (*Figure 2I*). Therefore, future studies should focus on developing a lumbar disc VR model.

Our study had a few limitations to note. First, the number of patients was small (n=53) due to the short duration of the study, and an approach with a larger patient group is required to reassess the results of our study. Second, an 8-week interval between image evaluations might have caused recall bias and statistical distortions.

Conclusions

ED images demonstrated superior diagnostic accuracy for detecting lumbar disc bulging, herniation, and spinal nerve root impingement as compared to VNCa and SC images. In addition, ED depicted disc calcification as effectively as did SC and will hopefully enable the development of a lumbar disc VR model. Therefore, ED could potentially become a viable alternative for visualizing lumbar disc disease.

Acknowledgments

None.

Footnote

Reporting Checklist: The authors have completed the STARD reporting checklist. Available at https://qims.amegroups.com/article/view/10.21037/qims-24-1760/rc

Funding: This work was supported by the Key Research and Development Program of Shaanxi Province (Nos. 2023-YBSF-074, 2023-YBSF-673, and 2017SF-081), the Scientific Research Projects of Xi'an Health Commission (No. 2021yb06), the Xi'an Central Hospital Science Foundation (No. 2023QN05), and the Science and Technology Program of Xi'an Grant (No. 23YXYJ0004).

Conflicts of Interest: All authors have completed the ICMJE uniform disclosure form (available at https://qims.amegroups.com/article/view/10.21037/qims-24-1760/coif). X.Z. is employed by Philips Healthcare, China. The other authors have no conflicts of interest to declare.

Ethical Statement: The authors are accountable for all aspects of the work in ensuring that questions related to the accuracy or integrity of any part of the work are appropriately investigated and resolved. This study was conducted in accordance with the Declaration of Helsinki (as revised in 2013) and was approved by the Institutional Review Board (IRB) of The Affiliated Xi'an Central Hospital of Xi'an Jiaotong University (No. LW-2024-04). The requirement for individual consent was waived due to the retrospective nature of the analysis.

References

1. Pan Q, Zhang K, He L, Dong Z, Zhang L, Wu X, Wu Y, Gao Y. Automatically Diagnosing Disk Bulge and Disk Herniation With Lumbar Magnetic Resonance Images by Using Deep Convolutional Neural Networks: Method Development Study. JMIR Med Inform 2021;9:e14755.
2. Porchet F, Wietlisbach V, Burnand B, Daeppen K, Villemure JG, Vader JP. Relationship between severity of lumbar disc disease and disability scores in sciatica patients. Neurosurgery 2002;50:1253-9; discussion 1259-60.
3. Zehra U, Tryfonidou M, Iatridis JC, Illien-Jünger S, Mwale F, Samartzis D. Mechanisms and clinical implications of intervertebral disc calcification. Nat Rev Rheumatol 2022;18:352-62.
4. Chanchairujira K, Chung CB, Kim JY, Papakonstantinou O, Lee MH, Clopton P, Resnick D. Intervertebral disk calcification of the spine in an elderly population: radiographic prevalence, location, and distribution and correlation with spinal degeneration. Radiology 2004;230:499-503.
5. Cheng XG, Brys P, Nijs J, Nicholson P, Jiang Y, Baert AL, Dequeker J. Radiological prevalence of lumbar intervertebral disc calcification in the elderly: an autopsy study. Skeletal Radiol 1996;25:231-5.
6. Cheng Y, Zhang Q, Li Y, Chen X, Wu H. Percutaneous

endoscopic interlaminar discectomy for L5-S1 calcified lumbar disc herniation: A retrospective study. Front Surg 2022;9:998231.
7. Choi JW, Lee JK, Moon KS, Hur H, Kim YS, Kim SH. Transdural approach for calcified central disc herniations of the upper lumbar spine. Technical note. J Neurosurg Spine 2007;7:370-4.
8. Dabo X, Ziqiang C, Yinchuan Z, Haijian N, Kai C, Yanbin L, Qiang F, Chuanfeng W. The Clinical Results of Percutaneous Endoscopic Interlaminar Discectomy (PEID) in the Treatment of Calcified Lumbar Disc Herniation: A Case-Control Study. Pain Physician 2016;19:69-76.
9. Street KJ, White SG, Vandal AC. Clinical prevalence and population incidence of serious pathologies among patients undergoing magnetic resonance imaging for low back pain. Spine J 2020;20:101-11.
10. Epstein NE, Hollingsworth RD. Nursing review of diagnosis and treatment of lumbar degenerative spondylolisthesis. Surg Neurol Int 2017;8:246.
11. Chappard C, Abascal J, Olivier C, Si-Mohamed S, Boussel L, Piala JB, Douek P, Peyrin F. Virtual monoenergetic images from photon-counting spectral computed tomography to assess knee osteoarthritis. Eur Radiol Exp 2022;6:10.
12. Chen M, Herregods N, Jaremko JL, Carron P, Elewaut D, Van den Bosch F, Jans L. Bone marrow edema in sacroiliitis: detection with dual-energy CT. Eur Radiol 2020;30:3393-400.
13. Gibney B, Murray N. Dual-Energy CT of Spinal Tophaceous Gout. Radiology 2020;296:276.
14. Ghazi Sherbaf F, Sair HI, Shakoor D, Fritz J, Schwaiger BJ, Johnson MH, Demehri S. DECT in Detection of Vertebral Fracture-associated Bone Marrow Edema: A Systematic Review and Meta-Analysis with Emphasis on Technical and Imaging Interpretation Parameters. Radiology 2021;300:110-9.
15. Booz C, Nöske J, Martin SS, Albrecht MH, Yel I, Lenga L, Gruber-Rouh T, Eichler K, D'Angelo T, Vogl TJ, Wichmann JL. Virtual Noncalcium Dual-Energy CT: Detection of Lumbar Disk Herniation in Comparison with Standard Gray-scale CT. Radiology 2019;290:446-55.
16. Koch V, Yel I, Grünewald LD, Beckers S, Burck I, Lenga L, Martin SS, Mader C, Wichmann JL, Albrecht MH, Eichler K, Gruber-Rouh T, D'Angelo T, Mazziotti S, Ascenti G, Vogl TJ, Booz C. Assessment of thoracic disk herniation by using virtual noncalcium dual-energy CT in comparison with standard grayscale CT. Eur Radiol 2021;31:9221-31.
17. Booz C, Yel I, Martin SS, Lenga L, Eichler K, Wichmann JL, Vogl TJ, Albrecht MH. Incremental Diagnostic Value of Virtual Noncalcium Dual-Energy Computed Tomography for the Depiction of Cervical Disk Herniation Compared With Standard Gray-Scale Computed Tomography. Invest Radiol 2021;56:207-14.
18. Mei K, Ehn S, Oechsner M, Kopp FK, Pfeiffer D, Fingerle AA, Pfeiffer F, Combs SE, Wilkens JJ, Rummeny EJ, Noël PB. Dual-layer spectral computed tomography: measuring relative electron density. Eur Radiol Exp 2018;2:20.
19. Nagano H, Takumi K, Nakajo M, Fukukura Y, Kumagae Y, Jinguji M, Tani A, Yoshiura T. Dual-Energy CT-Derived Electron Density for Diagnosing Metastatic Mediastinal Lymph Nodes in Non-Small Cell Lung Cancer: Comparison With Conventional CT and FDG PET/CT Findings. AJR Am J Roentgenol 2022;218:66-74.
20. Shim E, Kim BH, Kang WY, Hong SJ, Kang CH, Ahn KS, Lee H, Kwack TJ. Diagnostic performance of electron-density dual-energy CT in detection of cervical disc herniation in comparison with standard gray-scale CT and virtual non-calcium images. Eur Radiol 2022;32:2209-20.
21. Sudhyadhom A. On the molecular relationship between Hounsfield Unit (HU), mass density, and electron density in computed tomography (CT). PLoS One 2020;15:e0244861.
22. Brandelik SC, Skornitzke S, Mokry T, Sauer S, Stiller W, Nattenmüller J, Kauczor HU, Weber TF, Do TD. Quantitative and qualitative assessment of plasma cell dyscrasias in dual-layer spectral CT. Eur Radiol 2021;31:7664-73.
23. Fardon DF, Williams AL, Dohring EJ, Murtagh FR, Gabriel Rothman SL, Sze GK. Lumbar disc nomenclature: version 2.0: Recommendations of the combined task forces of the North American Spine Society, the American Society of Spine Radiology and the American Society of Neuroradiology. Spine J 2014;14:2525-45.
24. Pfirrmann CW, Dora C, Schmid MR, Zanetti M, Hodler J, Boos N. MR image-based grading of lumbar nerve root compromise due to disk herniation: reliability study with surgical correlation. Radiology 2004;230:583-8.
25. Notohamiprodjo S, Stahl R, Braunagel M, Kazmierczak PM, Thierfelder KM, Treitl KM, Wirth S, Notohamiprodjo M. Diagnostic accuracy of contemporary multidetector computed tomography (MDCT) for the detection of lumbar disc herniation. Eur Radiol 2017;27:3443-51.

26. van Rijn RM, Wassenaar M, Verhagen AP, Ostelo RW, Ginai AZ, de Boer MR, van Tulder MW, Koes BW. Computed tomography for the diagnosis of lumbar spinal pathology in adult patients with low back pain or sciatica: a diagnostic systematic review. Eur Spine J 2012;21:228-39.
27. Lee SM, Choo HJ, Lee SJ, Kim SK, Lee IS, Kim DW, Baek JW, Heo YJ. Cervical Spine CT Using Spectral Shaping: Can It Be a Solution to Overcome Artifacts in the Lower Cervical Spinal Region? Korean J Radiol 2019;20:469-78.
28. Novais EJ, Narayanan R, Canseco JA, van de Wetering K, Kepler CK, Hilibrand AS, Vaccaro AR, Risbud MV. A new perspective on intervertebral disc calcification-from bench to bedside. Bone Res 2024;12:3.
29. Shao J, Yu M, Jiang L, Wei F, Wu F, Liu Z, Liu X. Differences in calcification and osteogenic potential of herniated discs according to the severity of degeneration based on Pfirrmann grade: a cross-sectional study. BMC Musculoskelet Disord 2016;17:191.
30. Zhou J, Chen H, Yang T, Xing C, Jia F. Comparison of Predictive Ability of Computed Tomography and Magnetic Resonance Imaging in Patients with Carotid Atherosclerosis Complicated with Stroke. Iran J Public Health 2019;48:1052-8.
31. Wang Y, Cai A, Liang N, Yu X, Zhong X, Li L, Yan B. One half-scan dual-energy CT imaging using the Dual-domain Dual-way Estimated Network (DoDa-Net) model. Quant Imaging Med Surg 2022;12:653-74.
32. D'Angelo T, Albrecht MH, Caudo D, Mazziotti S, Vogl TJ, Wichmann JL, Martin S, Yel I, Ascenti G, Koch V, Cicero G, Blandino A, Booz C. Virtual non-calcium dual-energy CT: clinical applications. Eur Radiol Exp 2021;5:38.
33. Matos R, Fernandes PR, Matela N, Castro APG. Lumbar intervertebral disc segmentation for computer modeling and simulation. Comput Methods Programs Biomed 2023;230:107337.
34. Zheng G, Chu C, Belavý DL, Ibragimov B, Korez R, Vrtovec T, et al. Evaluation and comparison of 3D intervertebral disc localization and segmentation methods for 3D T2 MR data: A grand challenge. Med Image Anal 2017;35:327-44.

Cite this article as: Sun P, Wu X, Gao M, Zhang X, Ma D, Liu H, Zhang Q, Wu J, Ma M, Dong Y, Liu R. Improved visualization of electron-density dual-energy computed tomography for lumbar disc disease over the standard gray-scale type and virtual noncalcium imaging. Quant Imaging Med Surg 2025;15(3):2296-2308. doi: 10.21037/qims-24-1760

